

Technical note

# An experimental study of the surface drift currents in a wave flume

Zhenhua Huang\*

Department of Civil Engineering, The Hong Kong University of Science and Technology, Clearwater Bay, Kowloon, Hong Kong

Received 12 September 2005; accepted 16 January 2006

Available online 19 April 2006

## Abstract

The Lagrangian surface drift current induced by surface gravity waves in a wave flume has been investigated experimentally by the particle tracking method. It was observed that in most regions of the flume, the time-mean surface drift current was in the opposite direction to that of the wave propagation. The secondary current in the form of a pair of longitudinal vortices caused by the lateral boundaries was analyzed. It is suggested that the convection of the vorticity generated by the wave-absorber and the lateral boundaries is an important factor in the determination of the time-mean drift in a wave flume.

© 2006 Elsevier Ltd. All rights reserved.

*Keywords:* Surface waves; Mass transport; Time-mean current; Surface drift; Secondary current; Longitudinal vorticity

## 1. Introduction

Mass transport induced by surface water waves is a time-mean Lagrangian current. This steady streaming motion is generated by the wave-induced Reynolds stresses (Longuet-Higgins, 1953; Lighthill, 1978). The role played by the mass transport in the study of water waves and in the determination of the migration of sediment and pollutants in the water body is sufficiently important to justify further investigation of the subject. The time-mean surface drift is the wave-induced mass transport velocity on the mean water surface.

There is a rich literature in the theoretical study of mass transport in water waves, but there is a great discrepancy among the existing theories regarding the surface drift velocity and the profile of the mass transport velocity. Stokes (1847) in his classical memoir pointed out that individual water particles in irrotational, progressive waves did not have a closed path within one wave period. The water particles drift at a steady velocity (Stokes drift/mass transport velocity) of  $O(k\omega a^2)$  with  $\omega$  being the angular frequency,  $k$  the wave number and  $a$  the wave amplitude. In a semi-closed tank with a smooth bottom, the drift velocity on the mean water surface predicted by the

irrotational theory of Stokes (1847) is

$$\bar{u}_L(0) = \frac{\omega a^2 k}{2} \left[ \frac{\cosh(2kh)}{\sinh^2(kh)} - \frac{\coth(kh)}{kh} \right], \quad (1)$$

which is always positive (in the direction of wave propagation) for all dimensionless water depths  $kh$ .

Longuet-Higgins (1953) found that the small kinematic viscosity played a significant role in the determination of the mass transport velocity. He showed mathematically that the gradient of the Lagrangian drift velocity near the mean water surface was twice that of the corresponding value for the irrotational waves. In a semi-closed tank with a smooth bottom, the surface drift velocity predicted by this theory is

$$\bar{u}_L(0) = \frac{\omega a^2 k \coth(kh)}{kh} \left[ -\frac{3}{4} + \frac{k^2 h^2}{2} \right] + \frac{\omega a^2 k}{2 \sinh^2(kh)} \left[ -\frac{3}{4} + \cosh(2kh) \right] \quad (2)$$

(see also Craik, 1982). This surface drift velocity is positive (in the direction of the wave propagation) when  $kh > 0.694$  and negative (opposite to the direction of wave propagation) when  $kh < 0.694$ . In a semi-closed channel, the theories of Stokes (1847) and Longuet-Higgins (1953) give the same surface drift velocity when  $kh = 0.964$ . Ünlüata and Mei (1970) derived an equivalent expression for the mass transport velocity profile in Lagrangian coordinates,

\*Tel.: +852 23588763; fax: +852 23581534.

E-mail address: [cezh@ust.hk](mailto:cezh@ust.hk).

which is in agreement with that obtained by Longuet-Higgins (1953).

Recently, Gwinn and Jacobs (1997) developed a theory which considered the steady convection in a semi-closed wave flume. Based on this theory, the mass transport velocity gradually changes from a negative, uniform profile near the wave-maker to that of Longuet-Higgins (1953) in the region far away from the wave-maker. Comparisons with two stable velocity profiles of Mei et al. (1972) were performed. Groeneweg and Klopman (1998) developed a theory on wave-induced current changes in a general Lagrangian mean formulation, and also compared their results with two stable velocity profiles of Mei et al. (1972), but no consistent agreement between the theory and the experiments was reached under certain wave conditions.

All the theoretical studies mentioned above are for progressive waves in a single layer fluid over a rigid, smooth bottom. Recent progress in the theoretical study of the mass transport induced by perfect/partial standing waves over a smooth bottom can be found in Wen and Liu (1994) and Ng (2004). Wen and Liu (1994) also studied, as a special case, the 2-D convection solution of the mass transport in a rectangular wave flume when there was no reflection. They compared the numerical results with two measurements of Mei et al. (1972), and good agreement was found in the region near the wave-maker.

Even though there is a relatively rich literature in the experimental study of the wave-current interaction (A review of the available experimental data in this subject can be found in Huang and Mei (2003)), most experimental works on the mass transport in water waves focused on the near bed region, partially because of its importance in generating sand ripples and sand bars (see Ridler and Sleath, 2000 for a review in this subject). Available data on the mass transport velocity between the smooth bottom and the wave trough are given by Bagnold (1947), Russell and Osorio (1957), Mei et al. (1972), and Swan (1990). The mass transport velocity for progressive waves over a rough bottom can be found in Ridler and Sleath (2000). As expected, great discrepancy regarding the time-mean drift velocity profile and the time-mean surface drift exist among these data.

Using small particles as tracers, Russell and Osorio (1957) measured the velocity profile of the time-mean drift in a large closed channel. They found that wave breaking on the beach caused a strong backward drift on the surface (see also, Swan, 1990). To reduce this strong backward drift near the beach, a plastic curtain was installed in front of the pebble beach. They observed that the particles moved faster near the walls than away from the walls. The lateral drift velocity was not measured in their experiments, and no data showing the lateral variation of the longitudinal surface drift were reported. Mei et al. (1972) carried out their measurements several wavelengths away from the wave-maker. A dye tracing method was used to measure the mass transport velocity on the

central line and on a vertical plane 5 cm away from the sidewall. Most of their data were taken at a station 3.5 m away from the wave-maker. They also found that the mass transport velocity near the surface was faster near the walls than near the central line. Their measurements for  $0.9 \leq kh \leq 1.5$  agreed in general with the conduction solutions of Longuet-Higgins (1953). In some measurements, stable drift profiles could not be found even after the wave-maker had run for over 18 h. Swan (1990) measured, using laser Doppler anemometry (LDA), the vertical distribution of the Eulerian mass transport velocity above the wave bottom boundary layer and beneath the wave trough. He found that beneath the wave trough, the shear in the Eulerian mass transport velocity was negative, which was in dramatic contrast with positive shear predicted by the conduction solution of Longuet-Higgins (1953). Swan (1990) attributed the negative shear to the convection of the time-mean vorticity in the flume. It was suggested that the vorticity generated on the beach played an important role. Ridler and Sleath (2000) found that the maximum mass transport velocity near a rough bed could be either positive or negative, depending on the wave conditions. Their test section was just 1.7 m away from the beach. In all these studies, detailed time-history and the along/cross-channel variations of the longitudinal and lateral surface drift currents were not reported.

Craik (1982) argued that the drift current may be unstable to the lateral perturbation, leading to the formation of the longitudinal vorticity. The presence of the sidewall may produce the longitudinal vorticity as well (see, e.g., Huang and Mei, 2004). However, no experimental data are available to verify the above hypotheses. In flows dominated by waves of  $O(\omega a)$ , measuring both the time-history and spatial variation of the time-mean drift of  $O(k\omega a^2)$  is not an easy task with laser Doppler velocimetry (LDV) and traditional particle image velocimetry (PIV). As discrepancy among the predictions and measurements of the mass transport in a wave flume is more significant near the water surface, in this paper, we focus on the surface drift velocities, which are measured by using a particle tracking method. Attention is given to the time-history and the spatial variation of the 2-D surface drift velocity in a rectangular channel. Two types of the wave-absorbers are examined in the experiments. Both the longitudinal and the lateral drift velocities are investigated to reveal the wave-induced secondary current in the wave flume. Another aim of this paper is to reconcile the discrepancy in the existing data and theories, and provide a set of data to verify the existing mass transport theories and inspire the development of the new theories.

The findings in this paper are useful for problems such as wave-induced currents in long, narrow embayments where energy is dissipated near the shore and the swells at the entrance serve as the waves generated by the wave-maker.

## 2. Experimental set-up and procedure

### 2.1. The wave flume

The experiments were conducted in a glass-walled wave flume of 15.0 m in total length, 0.3 m in width and 0.5 m in depth. The section with the glass wall is 12.5 m long. A flap wave-maker was placed at one end and a wave-absorber at the other. Two types of wave-absorbers were used. The first wave-absorber (type A) was a permeable beach of slope 1:4, and the second one is the type A wave-absorber with a filter placed in front (type B). The experimental set-up and the two types of the wave-absorbers are shown in Fig. 1. Surface displacements along the flume were measured with resistance-type wave gages. Preliminary test showed that the reflection coefficients of these two types of the wave-absorbers were  $C_R = 9\%$  (type A) and  $C_R = 8\%$  (type B).

### 2.2. Measurement of the surface drift velocity

Let the  $x$ -coordinate be in the direction of the wave propagation and the  $z$ -axis vertically upwards with its origin at the still water level. The direction of the  $y$ -coordinate is determined by the right-hand rule. The origin of  $y$ -axis is located at the central line of the flume. The velocity components of a water particle on the moving water surface are defined by

$$u_L = \frac{dx(t)}{dt}, \quad v_L = \frac{dy(t)}{dt}, \quad w_L = \frac{dz(t)}{dt}, \quad (3)$$

where  $[x(t), y(t), z(t)]$  are the coordinates of the water particle on the moving water surface. The time-mean horizontal components  $\bar{u}_L$  and  $\bar{v}_L$  are defined by

$$\bar{u}_L = \frac{1}{T} \int_0^T \left( \frac{dx}{dt} \right) dt, \quad \bar{v}_L = \frac{1}{T} \int_0^T \left( \frac{dy}{dt} \right) dt, \quad (4)$$

where  $T$  is the wave period.  $[\bar{u}_L, \bar{v}_L]$  are the time-mean surface drift velocities on the mean water surface  $z = 0$ . The time-mean vertical drift velocity on the mean water surface is zero, i.e.,  $\bar{w}_L = 0$  at  $z = 0$ .

In a wave flume, the time-mean surface drift velocity (the time-mean Lagrangian velocity of a tracer on the mean water surface) can be measured by the particle tracking

method. In recording the movement of the tracers on the water surface, two lamps were used to illuminate the field of view. The motions of the tracers on the water surface are recorded and delivered to a computer by a digital camera at a rate of 25 frames per second. The distances traveled by the particles released at the same time were determined by two images obtained at a time interval  $\Delta t$  in the following way: first, one selects an instant  $t = t_1$  at which a chosen tracer is up-crossing the mean water surface. This instant is easily identified because it is at this instant that the tracer is about to reverse its motion direction. The image at this instant is called *Image 1*. Next the image at the instant  $t_2 = t_1 + nT$ , i.e.,  $\Delta t = nT$  (the integer  $n$  is normally taken to be 6 here) is found. This image is called *Image 2*. From these two images, the coordinates  $[x_1, y_1]$  of a tracer in *Image 1* and the coordinates  $[x_2, y_2]$  of the same tracer in *Image 2* are determined by discretizing the image. Finally, the time-mean surface drift velocities of the tracer are determined by (4)

$$\bar{u}_L(x_1, y) = \frac{x_2 - x_1}{\Delta t}, \quad \bar{v}_L(x_1, y) = \frac{y_2 - y_1}{\Delta t}, \quad y = \frac{y_1 + y_2}{2}. \quad (5)$$

The spatial resolution of the digital image was about 1mm/pixel in both  $x$  and  $y$  directions. The relative error in the time-mean surface drift can be estimated by

$$\left| \frac{\Delta \bar{u}_L}{\bar{u}_L} \right| \leq \left| \frac{\delta x}{\Delta x} \right| + \left| \frac{\delta t}{\Delta t} \right|, \quad (6)$$

where  $\delta t$  and  $\delta x$  are, respectively, the error in the measurement of the time interval  $\Delta t$  and the error in the measurement of the distance interval  $\Delta x$ . In the method discussed above, the error in measuring the distance is  $\delta x = O(1\sim 2)$  mm and the error in measuring the time interval is  $\delta t = O(1/25)$  s. For  $\bar{u}_L = O(10)$  mm/s and  $\Delta x = 5$  cm, the maximum relative error is less than  $O(5\%)$ , which is dominated by the error in the measurement of  $\Delta x$ . As  $\bar{v}_L$  is smaller than  $\bar{u}_L$ , the relative error in  $\bar{v}_L$  is larger than that in  $\bar{u}_L$ . In general, the error in the surface drift velocity is less than 10%, which is about the same as that for LDA for a typical time-mean drift velocity of 10 mm/s (see Ridler and Sleath, 2000).

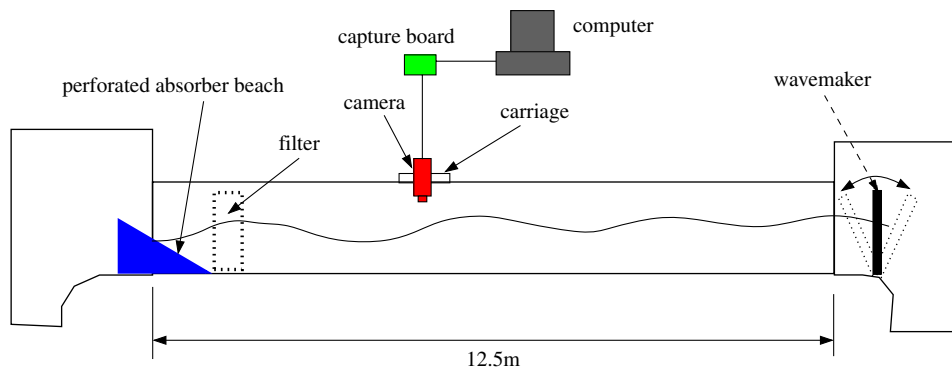


Fig. 1. Sketch of the experimental set-up.

Three types of tracers were examined, namely plastic rings, paper disks and black ink. The small plastic rings had an inner diameter of 2.5 mm and an outer diameter of 4 mm. The thickness of these small rings was about 1 mm. A dye method was also used to measure the surface drift, and the black ink used in this experiment was the brand Paperman. The paper disks were of diameter 5 mm, and were produced by using a hole-puncher. It was found that the three methods gave consistent results with a relative error within the accuracy of the methods used here. In this study, the small plastic rings were adopted as tracers to produce the results reported in this paper.

### 2.3. Test procedure

The water depth was fixed at  $h = 0.2$  m. The wave amplitude was  $a = 0.024$  m at the middle portion of the flume and the wave period  $T = 1$  s. Based on the linear dispersion relationship, the wave number was  $k = 5.15 \text{ m}^{-1}$ , which gave  $kh = 1.03$  and wave slope  $ka = 0.12$ . The wave period was determined by two methods. First it was measured with a stopwatch by counting 100 waves, and then calculated by a FFT analysis from the record of the surface displacement. By visual inspection of several tracers placed on the water surface, it was found that no residual drift existed in the flume after the water had been resting for about 30 min. In all the test runs reported in this paper, the wave-maker was started after the water had been resting for at least 60 min.

Surface drifts were measured at six test sections located at the following positions along the flume,  $x[\text{m}] = [1.0, 2.6, 4.6, 6.6, 8.6, 10.0]$ , where  $x$  was measured from the toe of the wave-absorber. The last test section ( $x = 10.0$  m) was located 2.2 m away from the wave-maker and the first test section  $x = 1.0$  m was located 11.2 m away from the wave-maker.

To reveal the variation of the time-mean surface drift velocity across the channel, about 10 tracers were released simultaneously along a straight line parallel to the wave crest at each test section. The motion of the tracers on the water surface was recorded at different time intervals until a steady state was reached. Preliminary tests showed that the steady state could be reached in about 30 min in this flume under the wave conditions encountered here.

All the tests were arranged into two stages. In the first stage, the time-mean surface drift was measured at each of the six test sections over a period of about 60 min. In the second stage, the time-mean surface drift was measured at the six test sections after the wave-maker had run for about 60 min and the steady state had been reached. The calculated time-mean surface drift velocities were then compared between these two stages to check the consistency of the drift current in the steady state. The difference was found to be within the accuracy of the method itself. The test procedure was the same for the two types of wave-absorbers used in this study.

## 3. Results and discussions

### 3.1. General features of the surface drift current

Fig. 2 is the time-mean surface drift measured at  $x = 2.6$  m from the toe of the wave-absorber (type A). As shown in the figure, the surface drift has two components: the longitudinal component  $\bar{u}_L$  and the lateral component  $\bar{v}_L$ .

#### 3.1.1. Longitudinal time-mean surface drift velocity

Initially the longitudinal time-mean surface drift  $\bar{u}_L$  is positive (in the direction of the wave propagation). In time, the longitudinal time-mean surface drift  $\bar{u}_L$  becomes negative (in the direction opposite to the wave propagation). Generally,  $\bar{u}_L$  is more or less uniform in the region

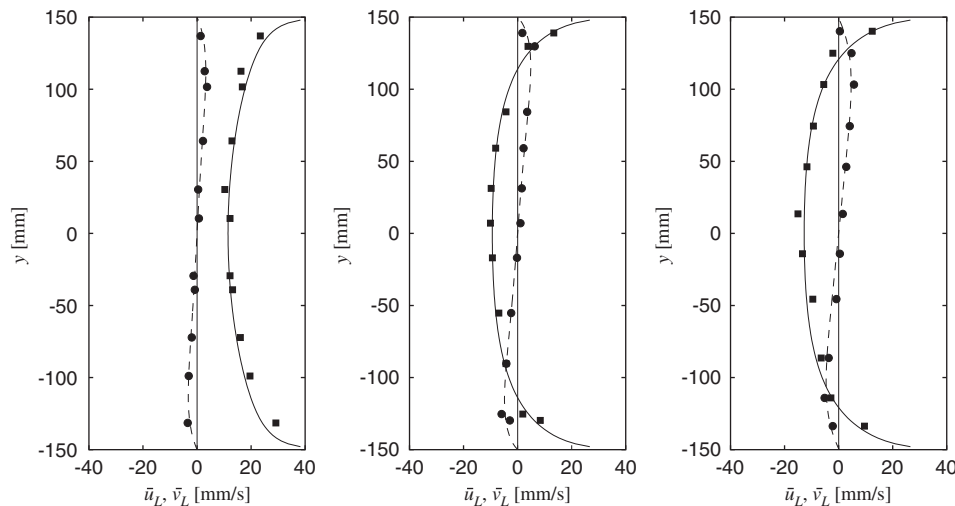


Fig. 2. Time-mean surface drift measured at  $x = 2.6$  m from the toe of the wave-absorber. From left to right:  $t = 30$  s, 5 and 60 min, respectively. Circles— $\bar{v}_L$ ; Squares— $\bar{u}_L$ . The solid- and dashed-lines are fitting curves based on (7) and (8), respectively. Test conditions:  $h = 20$  cm,  $T = 1$  s and  $H = 4.8$  cm.

close to the central line of the flume, but regions where  $\bar{u}_L$  has a relative large gradient exist next to the two sidewalls. These regions are not the wall boundary layers (the wall boundary layers due to the no-slip condition are not resolved by the present technique).

It was found that the longitudinal drift velocity  $\bar{u}_L$  was well represented by a curve of the form

$$\bar{u}_s = a_1(a_2 Y^4 + a_3 Y^2 + 1) \log\left(\frac{1 - Y^2}{a_4}\right), \quad (7)$$

where  $Y = 2y/W$  with  $W$  being the width of the flume. The nonlinear curve fitting can be easily performed by using the Matlab function `lsqcurvefit` to obtain the fitting parameters  $a_i$  ( $i = 1 \dots 4$ ), which are real. The curves corresponding to the empirical equation (7) have been included in Figs. 2, 4 and 7.

On the centerline ( $y = 0$ ), the time histories of the longitudinal time-mean surface drift velocity  $\bar{u}_L$ , measured at all the six test sections, are shown in Fig. 3. The longitudinal drift velocities on the centerline are calculated by a spline interpolation of the measured data points. It can be seen that  $\bar{u}_L$  gradually decreases with time from a positive value to a negative one (except at  $x = 10.0$  m). After a certain time,  $\bar{u}_L$  will approach a constant value, indicating that the steady state has been reached. At  $x = 1.0$  m, the time needed for  $\bar{u}_L$  to reach steady state is  $t \sim 400$  s. Fig. 3 shows that the time needed for  $\bar{u}_L$  to reach the steady state increases with the distance from the toe of the wave-absorber, suggesting that the change of the time-mean surface drift has to do with the convection of the vorticity from the wave-absorber to the entire flume (the time scale of the diffusion is much longer than 400 s).

### 3.1.2. Lateral time-mean surface drift velocity

As is shown in Fig. 2, a lateral time-mean surface drift velocity  $\bar{v}_L$  is always accompanied with the non-uniformity of  $\bar{u}_L$ . On the central line where  $\partial\bar{u}_L/\partial y = 0$ , the lateral time-mean surface drift velocity is zero ( $\bar{v}_L = 0$ ). Also  $\bar{v}_L$  is

zero on the two sidewalls due to the no-flux condition. In the region where  $\partial\bar{u}_L/\partial y > 0$ , the lateral time-mean surface drift velocity is positive ( $\bar{v}_L > 0$ ); while in the region where  $\partial\bar{u}_L/\partial y < 0$ , the lateral time-mean surface drift velocity is negative ( $\bar{v}_L < 0$ ). The magnitude of  $\bar{v}_L$  increases with time, and eventually reaches the steady state. Both  $\bar{u}_L$  and  $\bar{v}_L$  are of the same order, but numerically  $\bar{v}_L$  is smaller than that of  $\bar{u}_L$  ( $\max(\bar{v}_L) \sim 0.5 \max(\bar{u}_L)$ ) in Fig. 2). As discussed later in Section 3.3, the existence of the lateral drift  $\bar{v}_L$  will result in a secondary current in the wave flume.

It was also found that the lateral time-mean surface drift velocity  $\bar{v}_L$  was well represented by a curve of the form

$$\bar{v}_s = b_1[-(Y + 1)^{b_2} e^{-b_3(Y+1)} + (1 - Y)^{b_2} e^{b_3(Y-1)}], \quad (8)$$

where  $Y = 2y/W$  with  $W$  being the width of the flume. Again, the nonlinear curve fitting can be easily performed by using the Matlab function `lsqcurvefit` to obtain the fitting parameters  $b_i$  ( $i = 1 \dots 3$ ), which are real. The curves corresponding to the empirical (7) have also been included in Figs. 2, 4 and 7.

### 3.2. Time-mean surface drift current in steady state

When the wave-maker has run for about 1 h, the surface drift currents in the flume has already approached the steady state, as shown in Fig. 3. The distributions of the surface drift current at all six test sections are shown in Fig. 4. It can be seen that empirical equations (7) and (8) can satisfactorily fit the data. The longitudinal time-mean surface drift velocity  $\bar{u}_L$  was negative near the wave-absorber, and it gradually changed to a positive value near the wave-maker. The location where  $\bar{u}_L$  reverses its direction was between  $x = 8.6$  and  $10.0$  m, or about 2~4 wavelength away from the wave-maker. The lateral time-mean velocity  $\bar{v}_L$  also changed its sign when the longitudinal time-mean velocity  $\bar{u}_L$  did. Of course, at the mean location of the wave-maker, the time-mean surface drift has to be zero. At  $x = 1.0$  m,  $\bar{u}_L$  is approximately

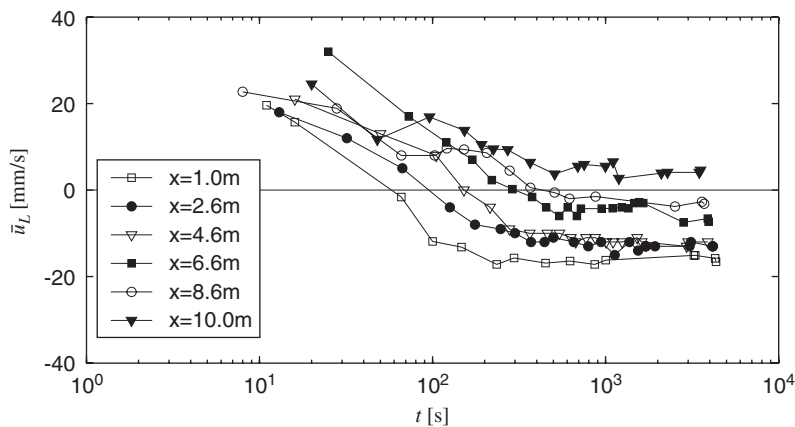


Fig. 3. Time history of the longitudinal time-mean surface drift velocity on the central line of the flume at all six test sections.  $x$  is measured from the toe of the wave-absorber.

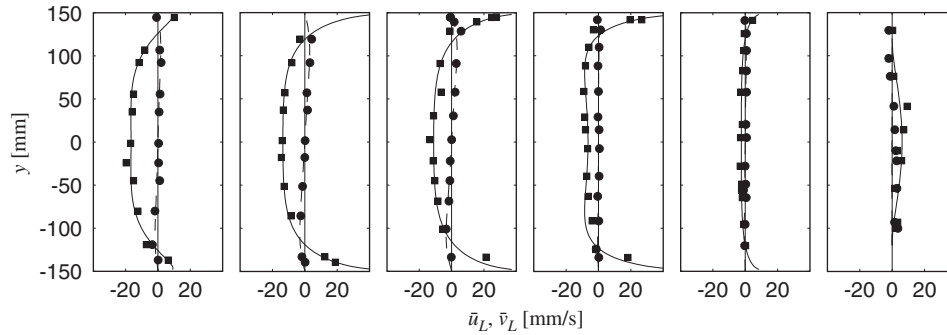


Fig. 4. The profiles of the time-mean surface drift current at all six test sections in the wave flume with type A wave-absorber. From left to right, respectively,  $x[m] = 1.0, 2.6, 4.6, 6.6, 8.6, 10.0$  away from the wave-absorber. Circles— $\bar{v}_L$ ; Squares— $\bar{u}_L$ . The solid- and dashed-lines are fitting curves based on (7) and (8), respectively. The wave-maker has run for 60 min.

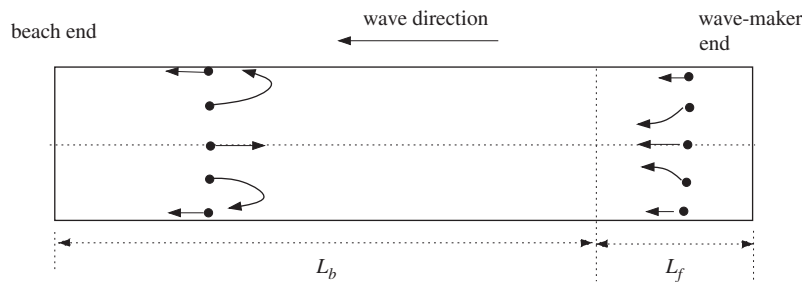


Fig. 5. Paths of the tracers on the water surface.

uniform between  $y = [-60 \text{ mm}, 60 \text{ mm}]$ ; while in the middle of the flume  $\bar{u}_L$  is approximately uniform between  $y = [-100 \text{ mm}, 100 \text{ mm}]$ . In general the time-mean drift current induced by waves in a flume has a significant spatial variation along the wave flume.

### 3.3. Secondary current in the wave flume

As has been shown, the lateral time-mean surface drift  $\bar{v}_L$  exists in the flume. This lateral drift current has an important impact on the general pattern of the drift current in the flume.

#### 3.3.1. Tracer path

Because of the lateral time-mean drift velocity  $\bar{v}_L$ , tracers on the water surface were observed to collect into lines next to the sidewalls in the region away from the wave-maker, but to collect at the centerline in the region near the wave-maker, as shown in Fig. 5. Let  $L_b$  be the length of the region where the time-mean surface drift current at the centerline is negative, and  $L_f$  the length of the region where the time-mean surface drift current at the centerline is positive. As expected, the ratio of  $L_b/L_f$  changes with time. At  $t \sim 60 \text{ min}$ ,  $L_b/L_f \sim 4$  under the wave conditions considered here. The picture shown in Fig. 5 can be viewed as an representation of the wave-induced current in a long, shallow embayment where the beach is the energy dissipater and the swells at the entrance serve as the waves

generated by a wave-maker. Thus in the absence of the wind-driven current and the tidal current, the motion in the embayment is driven by the swells, and materials floating on the water surface should move toward the two banks.

#### 3.3.2. Secondary current just beneath the mean water surface

Before discussing the secondary current induced by waves, the relation between the Eulerian time-mean current  $\bar{u}_E$  and the Lagrangian time-mean current  $\bar{u}_L$  should be considered. The time-mean current measured by a fixed probe is the Eulerian time-mean current which is related to the Lagrangian time-mean current  $\bar{u}_L$  by

$$\bar{u}_E(x, y, z) = \bar{u}_L(x, y, z) - U_s(z), \quad U_s = \frac{\omega k a^2 \cosh(2k(h+z))}{2 \sinh^2(kh)}, \quad (9)$$

where  $U_s(z)$  is the Stokes drift induced by long-crested surface waves (see e.g., Phillips, 1977; Mei, 1989). As waves are assumed to propagate in the  $x$ -direction, the Eulerian time-mean velocity  $(\bar{v}_E, \bar{w}_E)$  and the Lagrangian time-mean velocity  $(\bar{v}_L, \bar{w}_L)$  on the  $(y, z)$  plane are the same, i.e.,

$$\bar{v}_E(x, y, z) = \bar{v}_L(x, y, z), \quad \bar{w}_E(x, y, z) = \bar{w}_L(x, y, z). \quad (10)$$

The longitudinal variation of  $\bar{u}_L$  occurs over a length scale much longer than the water depth, the wave length and the width of the flume, thus the continuity equation

of the time-mean Eulerian drift current can be approximated by

$$\frac{\partial \bar{v}_E}{\partial y} + \frac{\partial \bar{w}_E}{\partial z} = 0. \tag{11}$$

The mean vertical velocity  $\bar{w}_E$  is zero on the mean water surface. According to the continuity equation (11), in the region where  $\partial \bar{v}_E / \partial y > 0$ , we must have  $\partial \bar{w}_E / \partial z < 0$  on the mean water surface and  $\bar{w}_E > 0$  adjacent to the mean water surface. Similarly, in the region where  $\partial \bar{v}_E / \partial y < 0$ , we must have  $\partial \bar{w}_E / \partial z > 0$  on the mean water surface and  $\bar{w}_E < 0$  adjacent to the mean water surface, as shown in Fig. 6. Therefore, there exists a secondary current induced by waves in the wave flume. Based on the analysis given

above, the secondary current just beneath the mean water surface is shown in Fig. 6 for the region close to the wave-absorber. It can be seen that the secondary current should take the form of a pair of longitudinal vortices.

The sign of the longitudinal vortices adjacent to the mean water surface can be determined by the following simple argument. The surface is free of stress, so on the mean water surface ( $z = 0$ ) the lateral shear stress is zero  $\partial \bar{v}_E / \partial z = 0$ . It is reasonable to assume that there is no rapid change in the shear stress adjacent to the mean water surface. As a result, the longitudinal vorticity  $\Omega_x \approx \partial \bar{w}_E / \partial y$  is positive in the region where  $\bar{v}_E < 0$  and negative in the region where  $\bar{v}_E > 0$ , as shown in Fig. 6. The longitudinal vortices shown here are not likely due to the instability, but more likely due to the vertical vorticity generated by the two sidewalls (Wen and Liu, 1994; Huang and Mei, 2004). To rule out the possible contribution from the instability, a much wider flume is needed. As the longitudinal vorticity can bring materials in water up and down, the existence of the longitudinal vorticity has great impact on the vertical mixing in channels such as a long, narrow embayment.

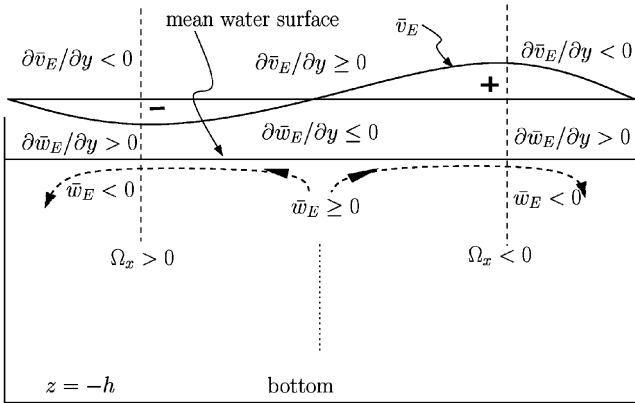


Fig. 6. The secondary velocity beneath the mean water surface in a region near the wave-absorber. Waves propagate vertically out of the paper.  $y$ -axis points from left to right.  $z$ -axis points upwards.

### 3.4. On the effect of the type of wave-absorber and the convection of vorticity

Dye was first used to study the nature of the flow in the flume. As soon as the dye was injected into the water 5 cm away from the wave-absorbers (both for types A and B), it lost its identity by violent mixing, indicating that the flow in this region is highly turbulent. However, the dye injected into water 50 cm away from the wave-absorbers was

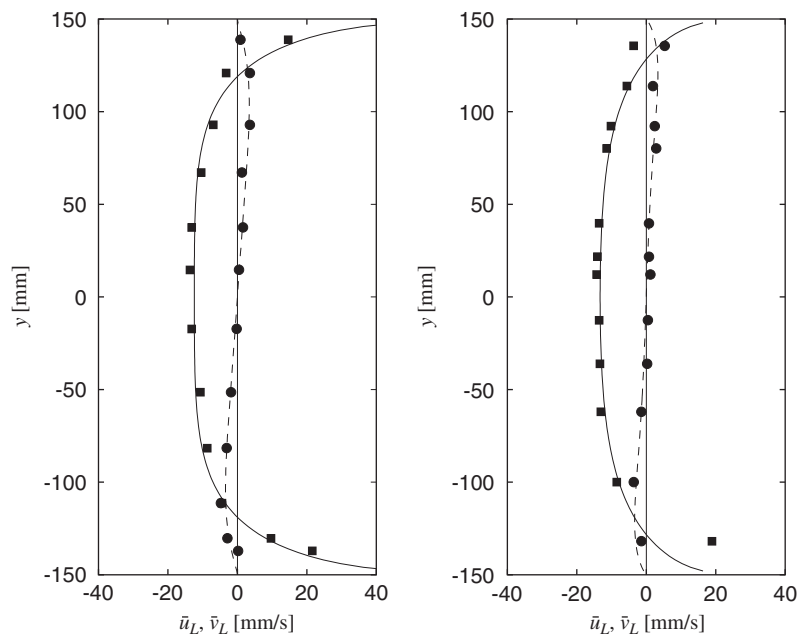


Fig. 7. The profiles of the surface drift at  $x = 2.6$  m for the two types of wave-absorbers. Squares— $\bar{u}_L$ ; Circles— $\bar{v}_L$ . The solid- and dashed-lines are fitting curves based on (7) and (8), respectively. The wave-maker has run for 60 min.

observed to be able to preserve its identity for at least tens of wave cycles before it lost its identity mainly by diffusion, indicating that the flow in the region far away from the wave-absorbers is possibly laminar.

To investigate the effect of the types of the wave-absorber on the time-mean surface drift, the profiles of the drift velocity measured at  $x = 2.6\text{ m}$  from the wave-absorbers are shown in Fig. 7 for both types A and B wave-absorbers. The magnitude and lateral variation of the longitudinal and lateral time-mean surface drift velocities are basically the same for these two types of wave-absorbers, indicating that the type of wave-absorber does not affect the time-mean surface drift about two wavelengths away from the toe of the wave-absorber. The above conclusion can also be supported by the time history of the longitudinal time-mean surface drift velocity on the centerline at  $x = 2.6\text{ m}$  from the wave-absorbers, which are shown in Fig. 8 for the two types of the wave-absorbers.

Wave-absorbers are commonly used to reduce the energy of the reflected waves so that the waves in the flume are approximately progressive. Clearly the flows inside and near the wave-absorber are no longer laminar and irrotational. As wave energy is continuously dissipated by the wave-absorber, the vorticity generated at the wave-absorber is likely to be able to be convected throughout the entire flume if the time is long enough, as suggested by Swan (1990). It is reasonable to argue that the details of the rotational flow near the wave-absorber is dependent on the type of the wave-absorber, but sufficiently far away from the wave-absorber this dependency will become weaker. The above hypotheses are partially supported by the fact that the surface drift currents at  $x = 2.6\text{ m}$  away from the wave-absorbers (both types A and B) have an almost identical time history except in the initial stages, as shown in Fig. 8.

The convection of the vorticity generated by the wave-absorber and the sidewalls is complicated. Based on Craik and Leibovich (1976), in a wave–current system the three vorticity components ( $\Omega_x, \Omega_y, \Omega_z$ ) are

governed by

$$\frac{\partial \Omega_x}{\partial t} + \Omega_z \frac{\partial U_s}{\partial z} = \bar{u}_E \frac{\partial \Omega_x}{\partial x} + \bar{v}_E \frac{\partial \Omega_x}{\partial y} + \bar{w}_E \frac{\partial \Omega_x}{\partial z} + \nu \nabla^2 \Omega_x, \quad (12)$$

$$\frac{\partial \Omega_y}{\partial t} = \bar{u}_E \frac{\partial \Omega_y}{\partial x} + \bar{v}_E \frac{\partial \Omega_y}{\partial y} + \bar{w}_E \frac{\partial \Omega_y}{\partial z} + \nu \nabla^2 \Omega_y, \quad (13)$$

$$\frac{\partial \Omega_z}{\partial t} = \bar{u}_E \frac{\partial \Omega_z}{\partial x} + \bar{v}_E \frac{\partial \Omega_z}{\partial y} + \bar{w}_E \frac{\partial \Omega_z}{\partial z} + \nu \nabla^2 \Omega_z \quad (14)$$

for the long-crested wave field where  $\partial U_s / \partial y = 0$  and  $\partial U_s / \partial x = 0$ . In Eqs. (12)–(14),  $\nu$  is the constant kinematic viscosity. The second term on the left of (12) is related to the “vortex-force”, which is the result of wave–current interaction (see Craik and Leibovich, 1976). This term is able to generate the longitudinal vorticity  $\Omega_x$  from the vertical vorticity  $\Omega_z = \partial \bar{u}_E / \partial y$  due to the sidewalls. The vorticity generated at the wave-absorber will be convected along the flume by mass transport  $\bar{u}_E$  and across the flume by the wave-induced secondary current ( $\bar{v}_E, \bar{w}_E$ ). As the vorticity generated at the wave-absorber is convected along the flume, it will interact with the vorticity generated by the sidewalls. In view of the small kinematic viscosity  $\nu$ , the diffusion in this process is relatively weak except in the region near the boundaries. Thus, the time-mean drift in the main body of the wave flume is convective instead of diffusive.

The time scale of the vorticity convection can be estimated by

$$T_x = \frac{x}{\bar{u}_E} = O\left(\frac{x}{U_s}\right), \quad (15)$$

where the longitudinal drift current is assumed to be of the same order of magnitude as the Stokes drift  $U_s$ . Under the wave conditions considered here:  $a = 0.024\text{ m}$ ,  $k = 5\text{ m}^{-1}$  and  $\omega = 6.28\text{ s}^{-1}$ , Eq. (15) gives  $U_s \sim 0.02\text{ m/s}$  and  $T_x = O(130\text{ s})$  for  $x = 2.6\text{ m}$ . The estimated convection time scale  $T_x$  is in agreement with our measurements as shown in Fig. 8, where the time-mean surface drifts at  $x = 2.6\text{ m}$  reached the steady state at about  $t = 400\text{ s}$ . For  $x = 8.6\text{ m}$ , Eq. (15) gives  $T_x = O(430\text{ s})$  which is also in good agreement with our measurement as shown in Fig. 3,

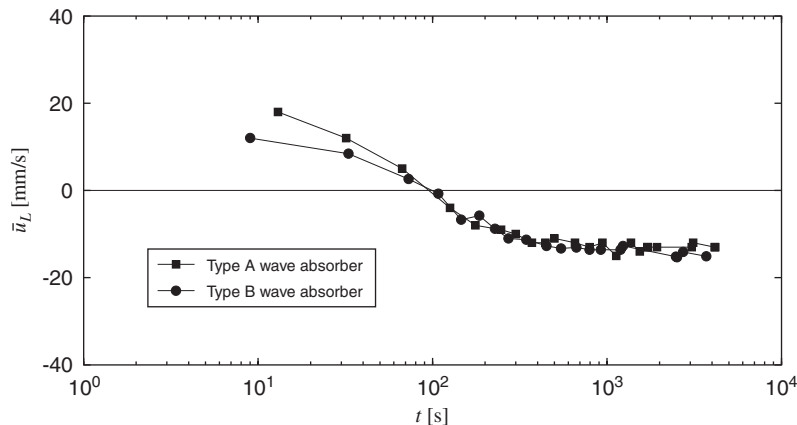


Fig. 8. Time history of the longitudinal time-mean surface drift velocity on the centerline at  $x = 2.6\text{ m}$  for two types of the wave-absorbers.

where the time-mean surface drift at  $x = 8.6$  m reached the steady state at about  $t = 600$  s.

It seems that the time-mean vorticity generated at the wave-absorber is the main cause of the negative surface drift current found in the region close to the wave-absorber, as Swan (1990) conjectured. It can be remarked from the experimental results that the time-mean vorticity generated at both the wave-absorber and the lateral boundaries are important in the formation and the convection of time-mean vorticity in the wave flume (or in semi-closed channels such as long, narrow embayments). As a result of the vorticity interaction and convection, the mass transport (and the time-mean surface drift) in the semi-closed channels has to be determined by solving the vorticity equations (12)–(14) with proper end and lateral boundary conditions.

3.5. On theories and experiments of mass transport in wave flumes

As shown in our experimental results, the time-mean surface drift in a wave flume varies along and across the flume. The time needed for the time-mean surface drift to reach the steady state is usually several hundreds of wave cycles. Same feature must also exist in the wave-induced mass transport (or drift) in a wave flume. It is not surprising to observe great discrepancy when the wave-induced drift measured at a particular position and time is compared with the theoretical predictions or other measurements.

The measured time-mean surface drift  $\bar{u}_L$  on the centerline is compared with the predictions of Eq. (1) (Stokes, 1847) and Eq. (2) (Longuet-Higgins, 1953), and the results are shown in Fig. 9. The measured time-mean surface drifts at all six test sections are smaller than both theoretical predictions. It can be seen that the discrepancy becomes more profound when the test section is closer to the wave-absorber. Mei et al. (1972) also found that the measured time-mean surface drift about 3.5 m away from the wave maker was positive and smaller than that calculated by

Longuet-Higgins (1953). The Fig. 5a in Swan (1990), showing the steady state Eulerian drift profile observed 3 m from the toe of the wave-absorber under the conditions  $h = 0.369$  m,  $a = 0.031$  m and  $\omega = 7.035$  s<sup>-1</sup>, gave the Lagrangian time-mean surface drift  $\bar{u}_L = \bar{u}_E + U_s \sim -5$  mm/s, which is in qualitative agreement with our observations in the regions close to the wave-absorbers.

Both Stokes (1847) and Longuet-Higgins (1953) assumed that waves propagate in an infinite domain, without a wave-maker, wave-absorber and the lateral boundaries. The theory of Gwinn and Jacobs (1997), who did consider the effect of the wave-maker, predicted the surface drift approaching that of Longuet-Higgins (1953) in a region far away from the wave-maker. Even though Gwinn and Jacobs (1997) considered the generation of the surface waves and convection in the flume, but their waves still propagate in an infinite long and wide channel, thus the vorticity generated by wave-absorber, sidewalls and wave-current interaction is not considered. It is noted that the vorticity equations (12)–(14) are similar to those used by Wen and Liu (1994), but their wave flume was infinitely long. Their numerical results revealed some basic features presented in this paper, for example, the existence of a wave-induced secondary current in a wave flume with a finite width (Figs. 9a and 10a in their paper). However, the effects of the wave-absorber was not taken into account in their theory.

4. Conclusions

In this research, the time-mean surface drift current in a wave flume was studied by a particle tracking method. The main conclusions are summarized as follows:

- (1) The steady-state surface drift was two-dimensional with variations both along and across the flume.
- (2) The longitudinal surface drift was negative in the region far away from the wave-maker, but positive near the wave-maker.

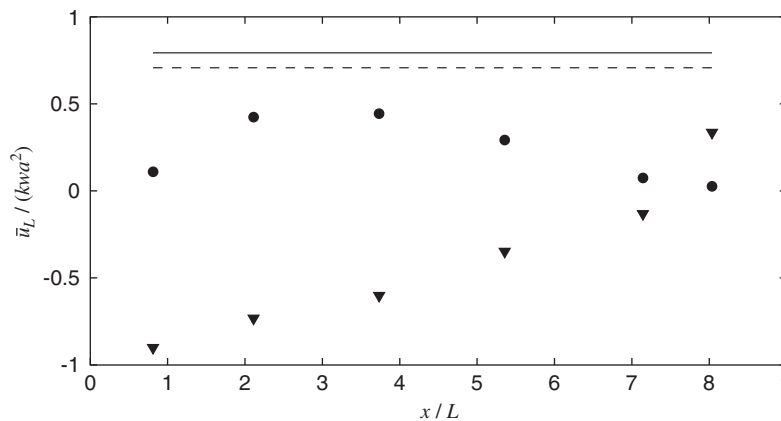


Fig. 9. Comparison between measurements and predictions. Solid line—Longuet-Higgins (1953); dashed-line—Stokes (1847); triangles— $\bar{u}_L$  measured at the centerline; solid circles— $\bar{u}_L$  measured 2 cm away from the sidewall.  $t = 60$  min.

- (3) The lateral variation of the longitudinal surface drift resulted in a secondary current near the mean water surface, in the form of a pair of longitudinal vortices.
- (4) The type of the wave-absorber had a weak effect on the evolution and the spatial distribution of the time-mean surface drift current, as long as the wave reflection coefficients of the wave energy dissipater are the same.
- (5) It was shown that the vorticity generated by the wave-absorber and sidewalls can be convected throughout the entire flume and that the convection determines the flow in the wave flume. It was conjectured that the wave energy dissipater (wave-breaking, wave-absorbers) was the main cause of the negative surface drift current near the wave-absorber.
- (6) It is suggested that the mass transport in the flume has to be determined by solving the full nonlinear vorticity equations (Wen and Liu, 1994) with the proper end and lateral boundary conditions. Efforts in this direction are being continued.

### Acknowledgments

This work was partially supported by University Grants Committee of the Hong Kong Special Administration Region under Grant DAG03/04.EG39.

### References

- Bagnold, R.A., 1947. Sand movement by waves: some small scale experiments with sand of very low density. *Journal of the Institution of Civil Engineers*, London 447–469.
- Craik, A.D.D., 1982. The drift velocity of water waves. *Journal of Fluid Mechanics* 116, 187–205.
- Craik, A.D.D., Leibovich, S., 1976. A rational model for langmuir circulations. *Journal of Fluid Mechanics* 73, 401–426.
- Groeneweg, J., Klopman, G., 1998. Changes of the mean velocity profiles in the combined waves-current motion in a GLM formulation. *Journal of Fluid Mechanics* 370, 271–296.
- Gwinn, A.W., Jacobs, S.J., 1997. Mass transport in viscous flow under progressive water wave. *Journal of Fluid Mechanics* 340, 61–82.
- Huang, Z., Mei, C.C., 2003. Effects of surface waves on a turbulent current over a smooth or rough seabed. *Journal of Fluid Mechanics* 497, 253–287.
- Huang, Z., Mei, C.C., 2004. Longitudinal vorticities in a water of finite depth in the absence of wind. In: Lee, J.H.W., Lam, K.M. (Eds.), *Environmental Hydraulics and Sustainable Water Management*. A.A. Balkema Publishers, London, pp. 121–126.
- Lighthill, M., 1978. *Waves in Fluids*. Cambridge University Press, Cambridge, MA.
- Longuet-Higgins, M., 1953. Mass transport in water waves. *Philosophical Transactions of the Royal Society of London* 245, 535–581.
- Mei, C.C., 1989. *The Applied Dynamics of Ocean Surface Waves*. World Scientific, Singapore.
- Mei, C.C., Liu, P.L.-F., Carter, T.G., 1972. Mass transport in water waves. Technical Report 146, Ralph M. Parsons Laboratory. Water Resources Hydrodynamics, MIT.
- Ng, C.-O., 2004. Mass transport in gravity waves revisited. *Journal of Geophysical Research* 109, C04012.
- Phillips, O.M., 1977. *The Dynamics of Upper Ocean*. Cambridge University Press, Cambridge, UK.
- Ridler, E.L., Sleath, J.F.A., 2000. Effect of bed roughness on time-mean drift induced by waves. *Journal of Waterway, Port, Coastal, and Ocean Engineering* 126 (1), 23–29.
- Russell, R.C.H., Osorio, D.C., 1957. An experimental investigation of drift profiles in a closed channel. In: *Proceedings of the Sixth Conference on Coastal Engineering*. ASCE, Miami, pp. 171–193.
- Stokes, G.G., 1847. On theory of oscillatory waves. *Transactions of the Cambridge Philosophical Society* 8, 441–455.
- Swan, C., 1990. Convection within an experimental wave flume. *Journal of Hydraulic Research* 28 (3), 273–282.
- Ünlüata, U., Mei, C.C., 1970. Mass transport in water waves. *Journal of Geophysical Research* 75 (36), 7611–7618.
- Wen, J., Liu, P.L.-F., 1994. Mass transport under partially reflected waves in a rectangular channel. *Journal of Fluid Mechanics* 266, 121–145.